Imaging the real shape of nanoclusters in scanning force microscopy

Olli H. Pakarinen,[1] Clemens Barth,[2,a)] Adam S. Foster,[1] and Claude R. Henry[2]

[1]*Laboratory of Physics, Helsinki University of Technology, P.O. Box 1100, FIN-02015 HUT, Finland*
[2]*CRMCN-CNRS, Campus de Luminy, Case 913, 13288 Marseille Cedex 09, France*

A quantitative comparison between experiment and theory is given for the constant height mode imaging of metal nanoclusters in dynamic scanning force microscopy. We explain the fundamental mechanisms in the contrast formation with the help of the system Pd/MgO(001). The comparison shows that the shape and size of nanoclusters are precisely imaged due to the sharpness of the tip's last nanometer. This quantitative comparison proves our previously proposed model for the contrast formation. © *2008 American Institute of Physics*. [DOI: 10.1063/1.2841700]

I. INTRODUCTION

Metal nanoclusters supported on oxide surfaces are very important model systems in nanocatalysis.[1–4] A key requirement for studying this kind of system, and generally in studies of nano-objects, is to be able to resolve the cluster in high spatial resolution with as fast a time resolution as possible. In order to locate the nanoclusters on the surface and to determine the cluster's size, shape, and internal structure, scanning probe microscopy (SPM) is used in most cases.[5–7] In particular, scanning force microscopy (SFM) is applied as soon as nanoclusters are supported on surfaces of insulating oxides such as magnesium oxide or aluminum oxide. In the latter case the topography of the nanoclusters is generally imaged in the contact mode of the force microscope,[8,9] where the imaging suffers under the tip-surface convolution effect[10]—due to the tip being comparable to the clusters in size, the clusters appear larger and more distorted in the images than in reality. The force microscope in its dynamic mode (dynamic SFM) offers the possibility to image surfaces with a true atomic resolution,[11–13] and indeed, to a greater extent in recent years, the dynamic SFM has been used for the imaging of nanoclusters on many types of surfaces.[14–24] However, also in dynamic SFM, the tip-surface convolution strongly reduces the resolution during imaging of the nanoclusters in the standard topography mode.[19,25,26] Furthermore, the scanning speed is limited and does not exceed speeds much higher than $\sim 1-2$ Hz, which does not permit time-dependent measurements on short time scales—a particular problem for biophysical SPM studies.[7,27]

The imaging of nanoclusters with high resolution and high scanning speeds is clearly missing and is of high interest not only in nanocatalysis but also in any area of surface science and nanotechnology. Recently, we have qualitatively shown that the lateral size and shape of nanoclusters can be more accurately imaged with high scanning speeds if the so-called *constant height mode* in dynamic SFM is used.[28] The constant height mode is similar to the one frequently used in scanning tunneling microscopy (STM),[29,30] and was already used for atomic resolution imaging in dynamic SFM.[31] It is a complementary mode to the topography mode

that permits imaging of the lateral dimensions of objects at nanometer and Angstrom scale.[23,31] In the constant height mode, the tip is scanned at a constant height above the surface with a high scanning speed of up to 50 Hz or more, where all information of the tip-surface interaction is included in images of the detuning Δf. We have shown that the nanoclusters appear rich in contrast and much sharper than in corresponding topography images, which is due to a much smaller tip-surface convolution effect in comparison to the one that appears in the topography imaging mode. In our recent work we anticipated that this is realized by a so-called *nanotip* that is located in the short-range interaction between the tip and cluster.[28]

In this paper we present a quantitative comparison between experiment and theory, which supports our assumptions. For the comparison the parameters of the cantilever oscillation (amplitude, spring constant, detuning) but also the parameters of the nanoclusters (size, shape, material) taken from experimental measurements were used as an input for theory. We performed dynamic SFM measurements on palladium nanoclusters grown on MgO(001) because it is an important model catalyst[1] and because it has a well-known geometry.[32,33] We achieved a good agreement between experiment and theory, which shows that the contrast can be indeed explained by the short-range interaction between the tip and cluster. By a more general analysis, we explain that the high-resolution constant height imaging of nanoclusters can be basically achieved as long as the last nanometer of the tip is *physically* or *chemically sharp*.

II. EXPERIMENT AND THEORY

A. Sample preparation

The sample was taken from commercial single MgO crystals of the highest available quality [4N purity, Pi-Kem (England)]. The surface was prepared by ultrahigh vacuum (UHV) cleavage at room temperature along the (001) cleavage plane. The crystal was then annealed in an UHV oven at 330 °C overnight in order to put the crystal into its equilibrium charge state.[34,35] Palladium clusters were then epitaxially grown by condensing a calibrated beam of neutral palladium atoms from a Knudsen cell on the surface at 390 °C. The cleavage, the deposition of palladium, and the scanning force imaging were done in the same UHV system.[34]

After the scanning force measurements, the replica method was used in order to analyze the nanoclusters by transmission electron microscopy (TEM).[36] A thin carbon film with a thickness of ~10 nm was evaporated on the Pd/MgO(001) surface in the same UHV chamber. Afterwards, the sample was extracted from the UHV chamber. The carbon film carrying the palladium deposit from the crystal surface was removed from the MgO substrate by lowering the crystal gently into a water-hydrogen chloride mixture (10% HCl). Parts of the carbon film could then be imaged with a JEOL 3010 high-resolution TEM.

B. Scanning force imaging

Dynamic SFM experiments were performed in the low 10^{-10} mbar pressure range and at room temperature with an Omicron STM/AFM. The setup of our SFM is described in references.[37–41] Dynamic SFM measures the change in frequency, Δf, that appears due to the interaction of the oscillating tip with the surface.[11,12] In order to measure the detuning with high precision and stability, we used a digital demodulator (EasyPLL, nanoSurf AG). A conducting silicon cantilever (p-Si, 0.015 Ω cm, Nanosensors) was excited to vibration at its resonance frequency of $f_0 = 67.8$ kHz ($k = 2.3$ N/m spring constant) with a peak-to-peak amplitude stabilized to $A_{p-p} = 12$ nm. Images were acquired with the Omicron SCALA system[40] and prepared with the help of the WSxM software.[42] A dark contrast in detuning (Δf) images corresponds to more negative detuning values and vice versa. With the help of Fig. 1, we give a brief overview of the imaging modes in dynamic SFM in the following. More details can be found in our recent work[28] and in Ref. 25.

In the so-called *topography mode* or *constant Δf mode*, the detuning Δf is kept constant by the distance control loop [Fig. 1(a)] on a preset value Δf_{preset} that is chosen by the user. In this imaging mode, the loop gain (LG) is high and the scanning speed v_{scan} low ($v_{scan} < 1-2$ Hz); changes in the detuning Δf are then on a time scale, which is similar to the time response τ of the integrator (I) and loop gain (LG). The tip follows the contours of the surface topography [pathway (1) in Fig. 1(b)]. All information of the tip-surface interaction is included in the topography image. In the *constant height mode* the loop gain and the scanning speed are considerably smaller and higher, respectively, so that the distance control loop is no longer capable of regulating on a constant detuning $\Delta f = \Delta f_{preset}$. The result is that the tip follows only partially the topography [pathways (2) and (3) in Fig. 1(b)] with an included memory effect of the tip pathway, leading to asymmetric cluster profiles along the fast scanning direction.[28] For very small loop gains and high scanning speeds, the tip follows only the inclination of the surface with respect to the fast scanning direction [pathway (4) in Fig. 1(b)]. The detuning image includes then all information of the tip-surface interaction, whereas the topography image shows only the inclined surface plane.

Constant height measurements are performed as follows: First, a couple of images are recorded in the topography imaging mode in the surface region of interest. During these measurements, the fast scanning direction (scanning line) is
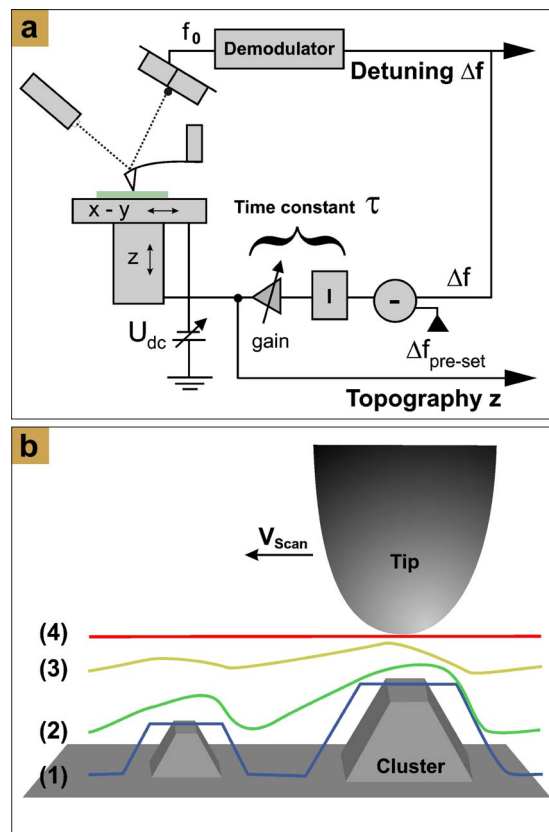

FIG. 1. (Color online) (a) The distance control loop in dynamic SFM. Note that the drawing is only a simplified diagram of the function principle. Detailed and precise circuits of the electronics can be found in Refs. 40 and 41. (b) Drawing explaining the differences between the constant Δf mode (1) and the constant height mode (4). Pathways (2) and (3) correspond to intermediate scanning conditions between both modes.

changed until it is parallel to the surface. No inclination between the fast scanning direction and the surface should be present. Afterward, a less negative value is chosen for the preset value Δf_{preset} so that the tip is put at a safe distance, far away from the surface. This can be done also during scanning. The loop gain is decreased to its smallest value and the scanning speed is increased (e.g., on 20 Hz). For the Omicron UHV STM/AFM, we choose a loop gain of 0.1% in the SCALA software.[40] Note that with the help of the digital demodulator (nanoSurf AG), the loop gain can be further linearly decreased by a factor of 10.[43] However, the total loop gain should be at least around 0.05% so that the tip is still capable of following the surface inclination during scanning. Optionally, a second-order low-pass filter at 300 Hz after the demodulator Δf output can be used in order to increase the sensitivity in Δf. After the loop gain and scanning speed have been adjusted, the preset value of the detuning is carefully decreased to more negative detuning values until a contrast is visible in the detuning image Δf.

Note that only the highest clusters are imaged in the constant height mode. However, this is not a restriction for smaller clusters, which are located in an adjacent surface region of the large clusters, because the scanning frame always can be chosen so that only the smaller clusters are actively scanned. The scanning characteristics of the constant height mode are then the same as in the case of the large clusters.

C. Calculations

In order to calculate the image contrast of Pd nanoclusters on the MgO(001) surface, we modeled the long-range interaction between the macroscopic bodies of the tip and surface. We built the tip and clusters from thin vertical cylinders (1×1 nm cross section) and summed the van der Waals interaction between them.[44] The Pd clusters were modeled in their expected shape of a truncated octahedron with an angle of 54.73° between the (001) top facet and the (111) side facets, and with a ratio of 0.45 between the cluster height and cluster base length.[32,33] The height and lateral size information was taken from the experimental topography and constant height images. Although it might be that the height of the nanometer-sized clusters is not well represented in dynamic SFM images,[25] we nevertheless used the cluster height values from our experimental images as guide values. It is a reasonable approximation in that the mechanism described in Ref. 25 is believed to be of almost the same strength for each cluster and therefore of small influence because the distribution of the cluster sizes can be assumed to be narrow. As a control, we checked the ratio between the cluster height and base length for some clusters and always found values around 0.45.

Since the silicon tip is originally exposed to the atmosphere, it is covered by an oxide layer. We therefore used a Hamaker constant of 15.60×10^{-20} J to represent the interaction of a silica tip with palladium.[45] In Fig. 2 we show the three different tip models used in the presented simulations: The first is the *sharp tip*, where the main part of the tip is a paraboloid with a radius of 5 nm and a height of 23 nm. Two other apexes were attached to the main part, each taking a radius of 2 nm. Side apexes have a lateral distance of $[+5, +5]$nm and $[-1, +5]$nm from the apex of the main tip. They are 0.9 and 0.8 nm higher than the apex of the main tip. The second *nanotip* model has the same shape at the lowest 1.5 nm of the apex, but a significantly blunter macroscopic part above that. The third *chemically sharp tip* has the same side apexes as the other tips, but the main apex is a blunt paraboloid tip with 25 nm radius, and in addition it has a minuscule nanotip, $1 \times 1 \times 0.2$ nm in size, with an additional short-range chemical interaction included. The short-range interaction is based on a TB-SMA (tight-binding second moment approximation) type of a potential,[46] which is a generic example of the short-range interaction that can be described with

$$E = Ae^{-p[(r_{ij}/r_0)-1]} - \xi\sqrt{e^{-2q[(r_{ij}/r_0)-1]}},$$

where $A = 7.38$ meV, $p = 6.40$, $\xi = 169$ meV, $q = 1.75$, and $r_0 = 0.3018$ nm. This chemical interaction remains below 30% of the total interaction and is based on first-principles calculations of the interaction between ionic tips and metal nanoclusters.[22]

Once the three-dimensional tip-surface force field has been calculated, it is included into a set of equations describing the cantilever dynamics[13] in order to calculate the detuning Δf of the cantilever oscillation frequency, i.e., a simulated image. In the calculations, the parameters describing the cantilever dynamics were taken from experiment (canti-
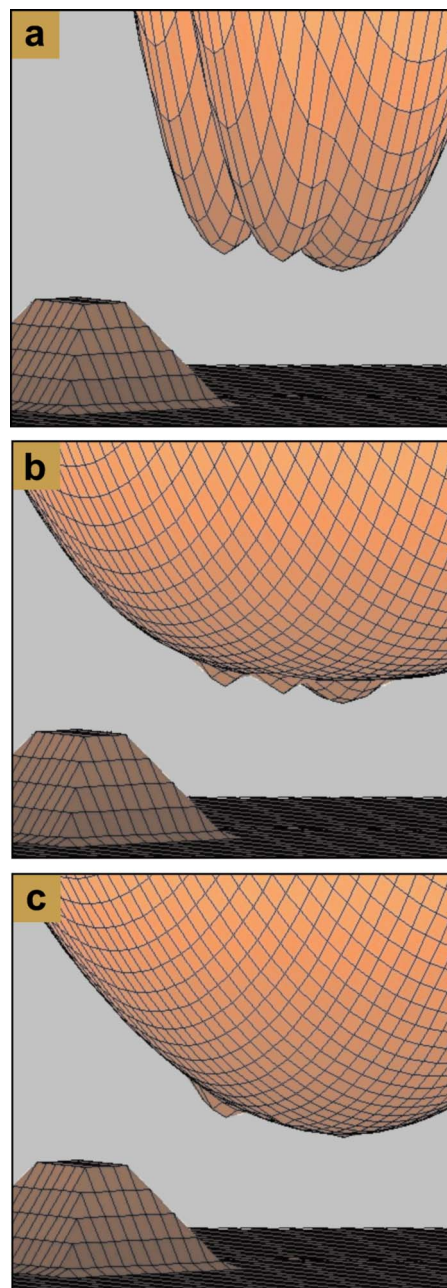

FIG. 2. (Color online) Three different tip models used for the simulations: sharp tip (a), nanotip model (b), and chemically sharp tip (c).

lever resonance frequency $f_0 = 67.8$ kHz, spring constant $k = 2.3$ N/m, and peak-to-peak amplitude $A_{\text{p-p}} = 12$ nm).

III. RESULTS

The transmission electron microscopy (TEM) images in Fig. 3 show well-known characteristics of Pd nanoclusters, which were grown *in situ* at 390 °C on a clean (001) surface of an UHV cleaved MgO single crystal. The Pd nanoclusters have a lateral rectangular shape, which generally can be observed by weak-beam dark-field TEM (Ref. 32) as exemplified by image (b) in Fig. 3. The lateral shape corresponds to a truncated octahedron which is the equilibrium 3D shape of the Pd nanoclusters on MgO(001) [image (c) in Fig. 3].[32,33] An important characteristic is also the angle of 45° between
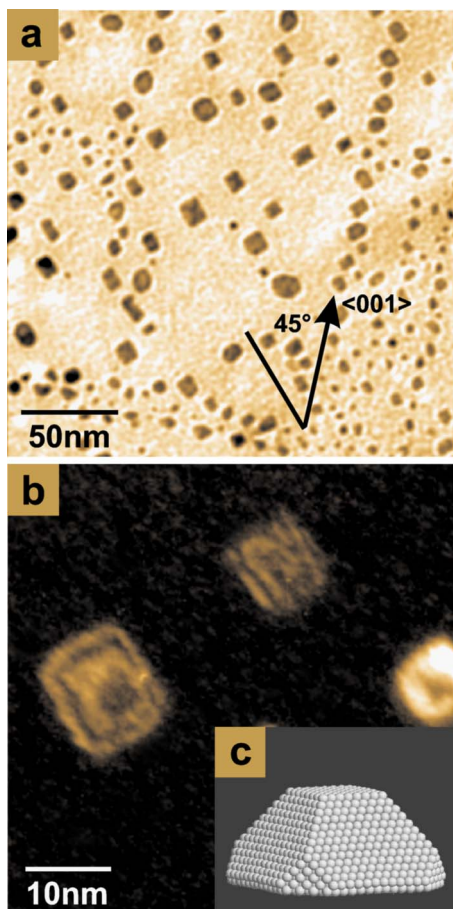
FIG. 3. (Color online) (a) Pd nanoclusters grown at 390 °C on a (001) surface of an UHV cleaved MgO crystal. The nominal thickness of Pd evaporated on the surface was 2 ML. The mean cluster density measured 4×10^{11} clusters/cm^2. (b) Weak-beam dark-field TEM image of large Pd nanoclusters. (c) Drawing of the expected 3D cluster shape (truncated octahedron).

the edges of the nanoclusters and ⟨001⟩ steps of the MgO(001) surface.[1,32]

Prior to TEM imaging, the same surface was imaged with the force microscope at room temperature after the deposition of Pd. The topography image in Fig. 4(a) shows single Pd nanoclusters with an apparent lateral size of some nanometers and apparent heights ranging between 3.8 and 6.4 nm. The image contrast of the nanoclusters is only of low quality: the lateral rectangular shape of the nanoclusters can only be roughly estimated. Furthermore, the nanoclusters seem to have an asymmetric shape, which can be seen in the profile in Fig. 4(b). The two angles of 34° and 18° do not coincide with the theoretical value of 54°73, which is the expected angle between the (001) top facet and the (111) side facets of a Pd nanocluster on MgO(001).[1] We imaged the same clusters in the constant height mode, which is shown in Fig. 4(c). During imaging we adjusted the tip-cluster distance by choosing a preset value of the detuning Δf in that only the top facets of the highest clusters at the ⟨001⟩ step were imaged. The image shows a strong contrast of the clusters, which is extremely sharp at the cluster edges. The profile in Fig. 4(d) shows that the contrast is formed by steep shoulders at the cluster edges and detuning values of up to

$\Delta f_{cluster} \approx -70$ Hz, which are much larger than the detuning values beside the clusters (∼−10 Hz). The main characteristic of the constant height image are the expected rectangular shapes of the clusters and the expected 45° orientation of the nanoclusters with respect to the ⟨001⟩ step of the MgO(001) surface.[32] A comparison of the cluster sizes in many of such constant height images with those of large clusters found in TEM images on the same sample surface shows a quantitative agreement.

Many of the clusters in the experimental image [Fig. 4(a)] show a similar arrangement of three peaks, the highest to the left, a smaller, roughly 1.0 nm lower peak 5 nm to the right, and a 1.1 nm lower peak 7 nm to the lower right. The indices 1–3 in Fig. 4(a) denote these three peaks in the topography image for one cluster on the surface. From the similar arrangement of peaks at each cluster at the ⟨001⟩ step [Fig. 4(a)], it is clear that these do not belong to the real shape of clusters on the surface, but they rather belong to an image of the tip produced by the tip-surface convolution.

To simulate the large-scale image presented in Fig. 4(a), we modeled the 20 most pronounced clusters which are visible in the experimental topography and constant height image [Figs. 4(a) and 4(c)], and simulated the imaging in the topography and constant height mode. As an input for the theory, the cluster heights were estimated from the experimental topography image, whereas the lateral cluster sizes were taken from both the experimental topography and constant height image. Since the experiments clearly suggest the presence of an asymmetric tip, we use the model of a *sharp* tip in the initial calculations (see Sec. II C).

The calculated topography and constant height image [Figs. 4(e) and 4(f)] are in a good agreement with the experimental results. The calculated topography image [Fig. 4(e)] shows the same characteristics as the experimental image [Fig. 4(a)]—both images show a strong convolution of the asymmetric macroscopic part of the tip with the nanoclusters, displaying a large number of apparent clusters caused by the side apexes of the tip. As an example, the shadow clusters 2 and 3 of cluster 1 in Fig. 4(a) are reproduced in the simulated image in Fig. 4(e). In contradiction to the calculated topography image, the calculated constant height image [Fig. 4(f)] shows a very strong contrast and a clear rectangular shape of the top facets of the clusters as in experiment. The real size of the clusters (top facets) is well represented in the calculated constant height image.

To compare experiment and simulations from a quantitative point of view, we considered a large series of images at different tip-surface distances of the three Pd clusters in the region of the gray dotted square shown in Fig. 4(a). Four images of the series are shown in Fig. 5. We decreased the tip-cluster distance from image to image by decreasing the preset value of Δf from −7.6 to −18.7 Hz [Figs. 5(a)–5(d)]. The image taken at the smallest negative detuning and therefore at the largest tip-cluster distance [Fig. 5(a)] shows a rather faint and fuzzy contrast of the three clusters. As the tip approaches the surface, the real shape of the clusters is quickly obtained, and their rectangular shape does not change much until the last image [Fig. 5(d)] (closest tip-cluster distance). Measurements at closer distances led to a
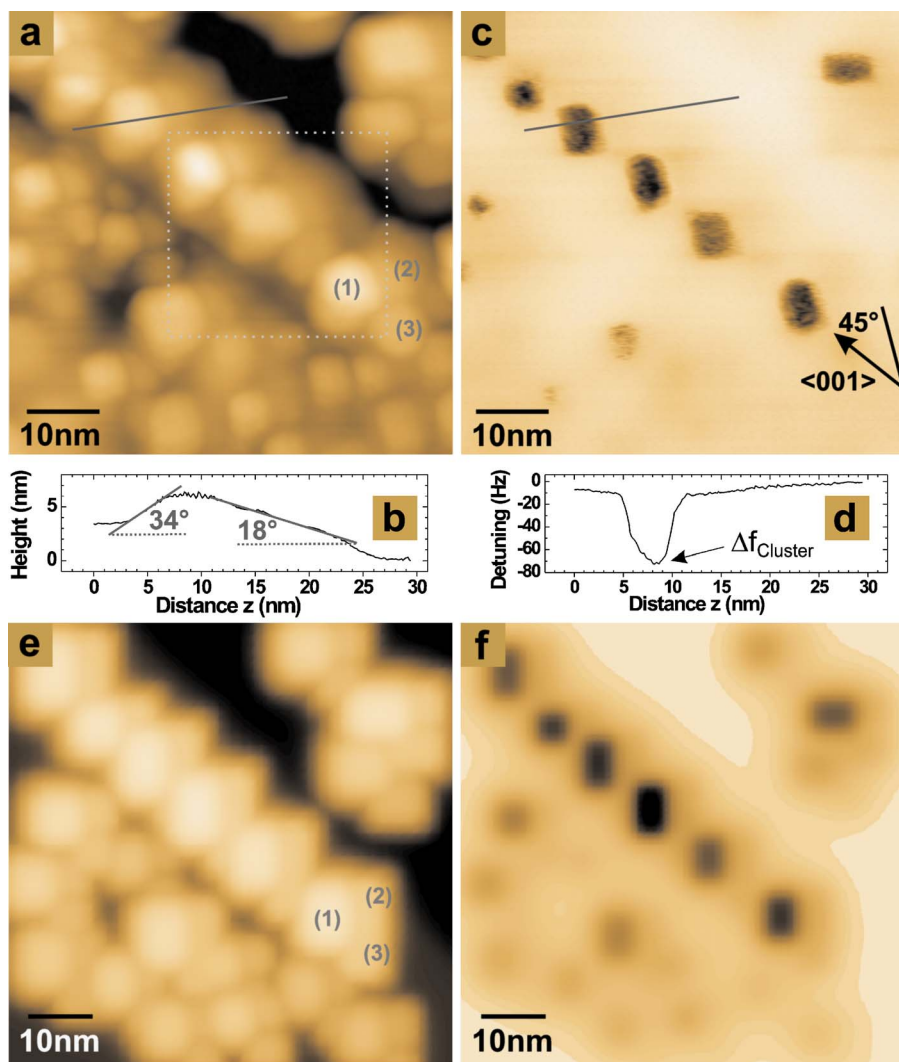
FIG. 4. (Color online) Experimental (a) and (c) and simulated images (e) and (f) of Pd nanoclusters on MgO(001) recorded or simulated in the topography (a) and (e) and constant height mode (c) and (f), respectively. The highest clusters, which are aligned in a row [e.g., in image (c)] are attached at a [001] step of the MgO(001) surface. (b),(d): Profiles taken at the positions of the gray lines in the experimental images (a) and (c). (a) 60×60 nm^2, $\Delta f = -41.2$ Hz, $v_{scan} = 2$ Hz; (c) 60×60 nm^2, $\Delta f_{mean} = -21.6$ Hz, $v_{scan} = 10$ Hz.

crash of the tip with the clusters. In Figs. 5(e)–5(h) calculated images of comparable clusters are shown. The shape and size of the clusters were estimated from the experimental images. The images were calculated at four different tip-cluster distances of 1.2 [Fig. 5(e)], 0.7 [Fig. 5(f)], 0.5 [Fig. 5(g)], and 0.4 nm [Fig. 5(h)]. These calculated images show the same details as the experimental images: at large distances the cluster contrast is fuzzy [Fig. 5(e)], whereas the clusters consecutively show their correct rectangular shapes with high contrast as soon as the tip gets close to the clusters [Figs. 5(e)–5(h)].

We analyzed the cluster contrast $\Delta f_{cluster}$ of each cluster in the experimental and theoretical images. The cluster contrast is shown in Fig. 6. As the tip-surface distance was unknown in the experiments, we fitted the experimental $\Delta f_{cluster}$ values of cluster 3 (green) by choosing the distance in the simulations such that the theoretical values well represented the experimental ones. This procedure is in fact a calibration of the tip-surface distance in the experiments. Following this, the $\Delta f_{cluster}$ values were calculated also for the other two clusters: cluster 1 (blue) and 2 (red). As can be seen, the cluster contrast of the other two clusters is rather well reproduced by theory for the complete distance range.

The good agreement between experiment and theory

shows that our model of contrast formation is correct. The main difference between the two imaging modes in Fig. 4 is that, if the tip follows the contours of the clusters in the topography imaging mode, also the side apexes of the tip interact with the clusters. They produce shadow images of clusters in the images and strongly reduce the resolution of the image. On the contrary, if the tip is scanned above the surface at a constant height [see Fig. 7], it is only the main part of the tip which is introduced into the minimum of the tip-cluster interaction, producing only one image per cluster, even when the height difference between the main apex and side apexes of the tip is less than 1 nanometer. In the topography mode the image is strongly affected by the shape and diameter of the tip from the apex at least to the height corresponding to the height of the surface features imaged, whereas in the constant height mode the image is mainly formed by the lowest nanometer of the tip (nanotip), which reduces the tip-surface convolution. The reason is that, in the topography mode, the height signal is following the tip profile linearly, whereas in the constant height mode, the interaction decrease is faster than linear when the tip-cluster distance increases.

Up to this point, we have considered only the van der Waals interaction between one tip and cluster. In an attempt
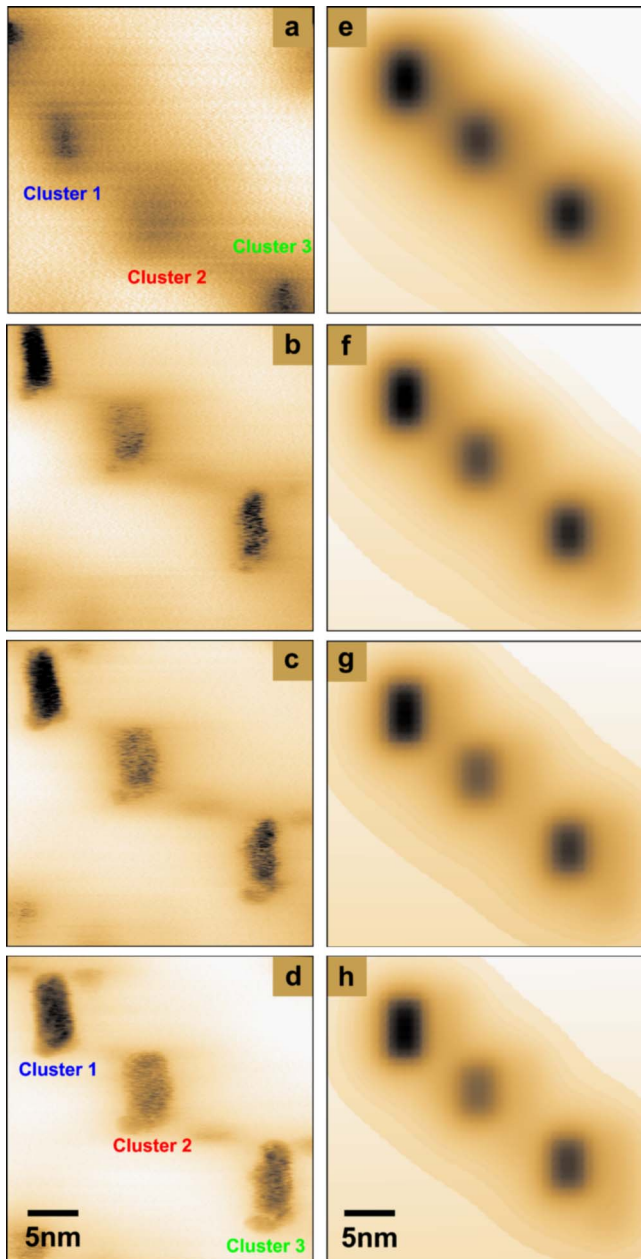
FIG. 5. (Color online) Experimental images (a)–(d) of three Pd clusters imaged in the region $(30 \times 30 \text{ nm}^2)$ of the dotted square in Fig. 4(a) and corresponding calculated images (e)–(h). The preset value of Δf was decreased during the measurements from image to image [−7.6 (a), −12.6 (b), −15.6 (c), and −18.7 Hz (d)]. Scan speed: $v_{scan} = 10$ Hz. The theoretical images (e)–(h) were calculated at the following tip-cluster distances: 1.2 (e), 0.7 (f), 0.5 (g), and 0.4 nm (h).

to generalize our results, we also investigated whether the same type of contrast can be principally gained with different types of short-range interactions or with so-called *nanotips* at the end of blunt tips. We tested a large number of different short-range potentials between the tip apex and the clusters, and we also considered very different tip configurations, including blunt tips presenting only a small nanotip to the surface. Although we did not get the same quantitative agreement between theory and experiment as in the specific van der Waals case presented above (Figs. 4–6), the same type of sharp cluster contrast can also be obtained with a macroscopically blunt tip, with either a sharp nanotip or significant
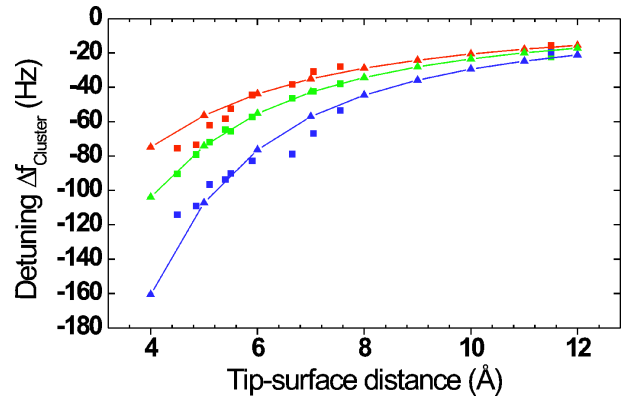

FIG. 6. (Color online) Distance-dependent contrast $\Delta f_{cluster}$ of all three clusters from Fig. 4 (experiment: ■; theory: continuous line).

short-range potential from the apex. Figure 8 shows a comparison between the three characteristic tip models introduced earlier—we emphasize that these tip models represent a small sample of the many tip models we considered, but we believe they cover the properties of a broad range of realistic tips. We can see that the constant height mode images retain their sharpness regardless of the bluntness of the macroscopic part of the tip, whereas the quality of the topographic mode images differs strongly with respect to the radius of the macroscopic part of the tip. This means that high-resolution constant height imaging of nano-objects can be achieved as long as the last nanometer of the tip is *physically* or *chemically sharp*.

IV. SUMMARY

In this paper we present a quantitative comparison between experiment and theory for the explanation of the contrast formation in constant height imaging of metal nanoclusters in dynamic SFM. In order to accomplish the comparison on a quantitative level, we used parameters of the cantilever oscillation and the size and shape of the clusters taken from the experimental measurements as an input for theory. The good agreement between experiment and theory in this spe-
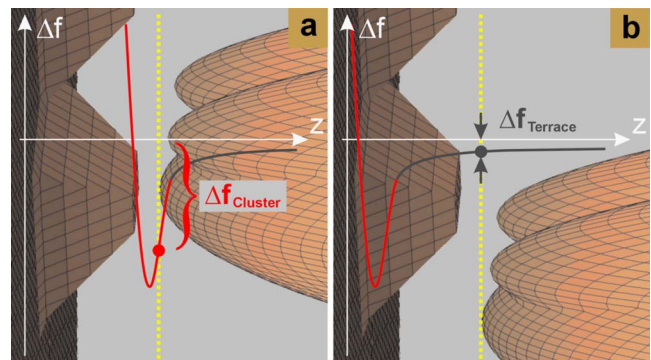

FIG. 7. (Color online) Drawing explaining the contrast formation in the constant height mode imaging of nanoclusters. The tip, which was used for the calculations, keeps a pathway with a constant height above the surface (yellow dotted line). (a) If the tip is above the cluster, it is only the last nanometer of the tip which is placed in the short-range interaction between tip and cluster, producing a large cluster contrast $\Delta f_{cluster}$. (b) As soon as the tip has passed the cluster, the tip is at a distance of the cluster height far away from the surface. The detuning value $\Delta f_{terrace}$ is then very small.
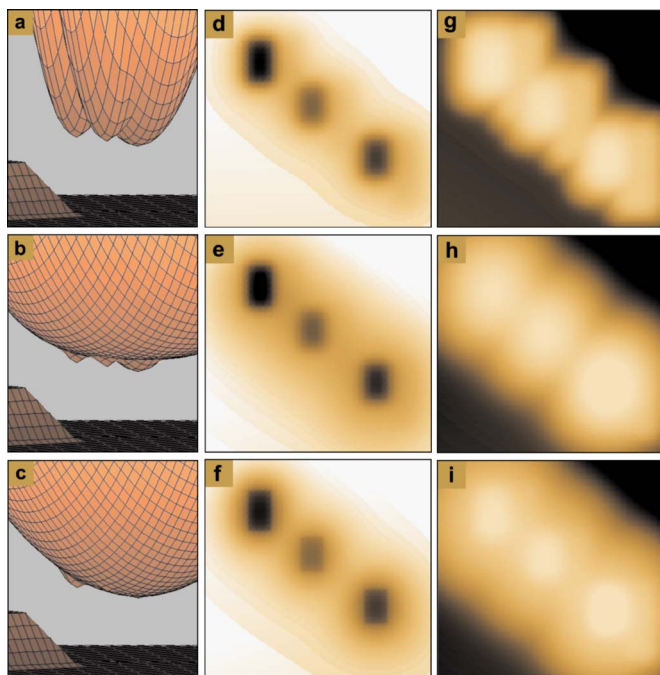
FIG. 8. (Color online) Three different tip models used for the simulations: sharp tip (a), nanotip model (b), and chemically sharp tip (c). Corresponding constant height mode (d)–(f) and topographic mode images (g)–(i).

cific case shows that the improved contrast can be explained by a short-range van der Waals interaction between the tip and cluster, and by the sharpness of the tip's last nanometer.

The work we present here strongly supports our previous assumptions,[28] and it basically shows that high lateral contrast of nanoclusters can be principally achieved as long as the last nanometer of the tip is physically or chemically sharp. Alongside the topography mode, which provides the height information of objects on the surface, the constant height mode can be used to precisely determine the lateral size and shape of nanoclusters. We also believe that many other types of nano-objects can be imaged in the constant height mode. Not only is the high contrast and the reduction of the tip-surface convolution beneficial, but also the scanning speed, which is only limited by the cantilever oscillation frequency. Our approach opens the door to the nanoscale in both lateral precision and time resolution in SFM studies of nano-objects.

ACKNOWLEDGMENTS

[1]C. R. Henry, Surf. Sci. Rep. **31**, 231 (1998).
[2]U. Heiz and U. Landman, *Nanocatalysis* (Springer-Verlag, Berlin, 2007).
[3]J. Libuda and H.-J. Freund, Surf. Sci. Rep. **57**, 157 (2005).
[4]K. P. McKenna, P. V. Sushko, and A. L. Shluger, J. Phys. Chem. C **111**, 2823 (2007).
[5]K. L. Yeung and N. Yao, J. Nanosci. Nanotechnol. **4**, 647 (2004).
[6]J. Loos, Adv. Mater. **17**, 1821 (2005).
[7]A. Alessandrini and P. Facci, Meas. Sci. Technol. **16**, R65 (2005).
[8]S. Ferrero, A. Piednoir, and C. R. Henry, Nano Lett. **1**, 227 (2001).
[9]K. Højrup-Hansen, S. Ferrero, and C. R. Henry, Appl. Surf. Sci. **226**, 167 (2004).
[10]S. Xu and M. F. Arnsdorf, J. Microsc. **173**, 199 (1994).
[11]S. Morita, R. Wiesendanger, and E. Meyer, *Noncontact Atomic Force Microscopy* (Springer-Verlag, Berlin, 2002).
[12]F. J. Giessibl, Rev. Mod. Phys. **75**, 949 (2003).
[13]W. A. Hofer, A. S. Foster, and A. L. Shluger, Rev. Mod. Phys. **75**, 1287 (2003).
[14]W. Mahoney, D. M. Schaefer, A. Patil, R. P. Andres, and R. Reifenberger, Surf. Sci. **316**, 383 (1994).
[15]J. V. Zoval, R. M. Stiger, P. R. Biernacki, and R. M. Penner, J. Phys. Chem. **100**, 837 (1996).
[16]T. R. Ramachandran, A. Madhukar, P. Chen, and B. E. Koel, J. Vac. Sci. Technol. A **16**, 1425 (1998).
[17]G. Haas, A. Menck, H. Brune, J. V. Barth, J. A. Venables, and K. Kern, Phys. Rev. B **61**, 11105 (2000).
[18]Z. Gai, G. A. Farnan, J. P. Pierce, and J. Shen, Appl. Phys. Lett. **81**, 742 (2002).
[19]C. Barth and C. R. Henry, Nanotechnology **15**, 1264 (2004).
[20]S. L. Tait, L. T. Ngo, Q. Yu, S. C. Fain, Jr., and C. T. Campbell, J. Chem. Phys. **122**, 064712 (2005).
[21]S. Kielbassa, A. Häbich, J. Schnaidt, J. Bansmann, F. Weigl, H.-G. Boyen, P. Ziemann, and R. J. Behm, Langmuir **22**, 7873 (2006).
[22]O. H. Pakarinen, C. Barth, A. S. Foster, R. M. Nieminen, and C. R. Henry, Phys. Rev. B **73**, 235428 (2006).
[23]C. Barth and C. R. Henry, Appl. Phys. Lett. **89**, 252119 (2006).
[24]M. Goryl, F. Buatier de Mongeot, F. Krok, A. Vevecka-Priftaj, and M. Szymonski, Phys. Rev. B **76**, 075423 (2007).
[25]S. C. Fain, Jr., C. A. Polwarth, S. L. Tait, C. T. Campbell, and R. H. French, Nanotechnology **17**, S121 (2006).
[26]J. Polesel-Maris, H. Guo, T. Zambelli, and S. Gauthier, Nanotechnology **17**, 4204 (2006).
[27]L. M. Picco, L. Bozec, A. Ulcinas, D. J. Engledew, M. Antognozzi, M. A. Horton, and M. J. Miles, Nanotechnology **18**, 044030 (2007).
[28]C. Barth, O. H. Pakarinen, A. S. Foster, and C. R. Henry, Nanotechnology **17**, S128 (2006).
[29]A. Bryant, D. P. E. Smith, and C. F. Quate, Appl. Phys. Lett. **48**, 832 (1986).
[30]R. Wiesendanger, *Scanning Probe Microscopy and Spectroscopy* (Cambridge University Press, Cambridge, UK, 1998).
[31]C. Barth, A. S. Foster, M. Reichling, and A. L. Shluger, J. Phys.: Condens. Matter **13**, 2061 (2001).
[32]H. Graoui, S. Giorgio, and C. R. Henry, Philos. Mag. B **81**, 1649 (2001).
[33]J. Goniakowski and C. Mottet, J. Cryst. Growth **275**, 29 (2005).
[34]C. Barth, C. Claeys, and C. R. Henry, Rev. Sci. Instrum. **76**, 083907 (2005).
[35]C. Barth and C. R. Henry, Nanotechnology **17**, S155 (2006).
[36]G. A. Bassett, Philos. Mag. **3**, 1042 (1958).
[37]G. Meyer and N. M. Amer, Appl. Phys. Lett. **53**, 1045 (1988).
[38]L. Howald, E. Meyer, R. Lüthi, H. Haefke, R. Overney, H. Rudin, and H.-J. Güntherodt, Appl. Phys. Lett. **63**, 117 (1993).
[39]T. R. Albrecht, P. Grütter, D. Horne, and D. Rugar, J. Appl. Phys. **69**, 668 (1991).
[40]Omicron GmbH, *The UHV AFM/STM User's Guide, The SPM SO V2.2 Software Manual*, SCALA Electronics, Technical Reference Manual (Omicron Vacuumphysik GmbH, Taunusstein, Germany, 1997–1998).
[41]G. Couturier, R. Boisgard, D. Dietzel, and J. P. Aimé, Nanotechnology **16**, 1346 (2005).
[42]I. Horcas, R. Fernández, J. M. Gómez-Rodríguez, J. Colchero, J. Gómez-Herrero, and A. M. Baro, Rev. Sci. Instrum. **78**, 013705 (2007).
[43]Nanosurf AG, *easyPLL, Reference Manual Version 2.2* (Nanosurf AG, Liestal, Switzerland, 2002).
[44]K. Cooper, A. Gupta, and S. Beaudoin, J. Colloid Interface Sci. **234**, 284 (2001).
[45]L. Bergström, Adv. Colloid Interface Sci. **70**, 125 (1997).
[46]N. I. Papanicolaou and D. A. Papaconstantopoulos, Thin Solid Films **428**, 40 (2003).